Article

Analysis and Optimization of Conditions for the Use of 2′,7′-Dichlorofluorescein Diacetate in Cultured Hepatocytes

Megan J. Reiniers [1,2], Lianne R. de Haan [1,3], Laurens F. Reeskamp [4], Mans Broekgaarden [5,6], Rowan F. van Golen [7,†] and Michal Heger [1,3,8,*,†]

1 Jiaxing Key Laboratory for Photonanomedicine and Experimental Therapeutics, Department of Pharmaceutics, College of Medicine, Jiaxing University, Jiaxing 314001, China; megan.reiniers@gmail.com (M.J.R.); dehaan.lianne@gmail.com (L.R.d.H.)
2 Department of Surgery, Haaglanden Medisch Centrum, 2512 VA The Hague, The Netherlands
3 Laboratory of Experimental Oncology, Department of Pathology, Erasmus MC, 3015 GD Rotterdam, The Netherlands
4 Department of Vascular Medicine, Amsterdam UMC, Location AMC, 1105 AZ Amsterdam, The Netherlands; l.f.reeskamp@amsterdamumc.nl
5 Team Cancer Targets and Experimental Therapeutics, Department Microenvironment Cell Plasticity and Signaling, Institute for Advanced Biosciences, CNRS UMR 5309, Université de Grenoble-Alpes, Allée des Alpes, 38700 La Tronche, France; mans.broekgaarden@univ-grenoble-alpes.fr
6 INSERM U 1209, Allée des Alpes, 38700 La Tronche, France
7 Department of Gastroenterology and Hepatology, Leiden University Medical Center, 2333 ZA Leiden, The Netherlands; R.F.van_Golen@lumc.nl
8 Department of Pharmaceutics, Utrecht Institute for Pharmaceutical Sciences, Utrecht University, 3584 CG Utrecht, The Netherlands
* Correspondence: m.heger@jctres.com or m.heger@uu.nl; Tel.: +86-138-19345926 or +31-30-2533966
† Shared senior authorship.

Abstract: Numerous liver pathologies encompass oxidative stress as molecular basis of disease. The use of 2′,7′-dichlorodihydrofluorescein-diacetate (DCFH$_2$-DA) as fluorogenic redox probe is problematic in liver cell lines because of membrane transport proteins that interfere with probe kinetics, among other reasons. The properties of DCFH$_2$-DA were analyzed in hepatocytes (HepG2, HepaRG) to characterize methodological issues that could hamper data interpretation and falsely skew conclusions. Experiments were focused on probe stability in relevant media, cellular probe uptake/retention/excretion, and basal oxidant formation and metabolism. DCFH$_2$-DA was used under optimized experimental conditions to intravitally visualize and quantify oxidative stress in real-time in HepG2 cells subjected to anoxia/reoxygenation. The most important findings were that: (1) the non-fluorescent DCFH$_2$-DA and the fluorescent DCF are rapidly taken up by hepatocytes, (2) DCF is poorly retained in hepatocytes, and (3) DCFH$_2$ oxidation kinetics are cell type-specific. Furthermore, (4) DCF fluorescence intensity was pH-dependent at pH < 7 and (5) the stability of DCFH$_2$-DA in cell culture medium relied on medium composition. The use of DCFH$_2$-DA to measure oxidative stress in cultured hepatocytes comes with methodological and technical challenges, which were characterized and solved. Optimized in vitro and intravital imaging protocols were formulated to help researchers conduct proper experiments and draw robust conclusions.

Keywords: fluorogenic redox probe; oxidative and nitrosative stress; liver diseases; hepatocytes; cellular uptake and export; intravital fluorescence imaging; anoxia and reoxygenation

1. Introduction

Oxidants in the form of reactive oxygen and nitrogen species (ROS and RNS, respectively), redox-active transition metals such as Fe^{2+} and Cu^+, as well as activated peroxidases (e.g., cytochrome c peroxidase) are chemically reactive compounds that are able to (ir)reversibly alter the structure of (bio)molecules [1]. ROS/RNS are generated

intracellularly by enzymatic sources (e.g., cytochrome P450 enzymes [2]) as well as non-enzymatic sources (e.g., oxidative phosphorylation in mitochondria [3]) and are essentially involved in cell signaling pathways when formed under controlled conditions. Transition metals are generally kept in a protein-bound state to control their reactivity, although a labile pool of free Fe^{2+} and Cu^+ exists intracellularly and is maintained within tight concentration limits under non-pathological circumstances [4]. Under pathological circumstances, however, oxidant levels can rise due to the increased formation of ROS/RNS, augmentation of the labile Fe^{2+}/Cu^+ pool, and/or a reduction in the (extra)cellular antioxidative capacity. A state of oxidative stress consequently ensues [1] that has been causally related to, e.g., cardiovascular-, neurodegenerative-, malignant-, and liver diseases [5]. Hepatocytes are particularly prone to developing oxidative stress because of their large number of mitochondria and ROS/RNS-producing enzymes, as well as their principal role in copper and iron metabolism [1]. Accordingly, oxidative stress contributes to many forms of liver disease [1,6] and therefore constitutes a major research topic within the field of hepatology.

Because of their high reactivity and short half-lives oxidants are difficult to measure directly, particularly under in vitro conditions. Consequently, fluorogenic and luminogenic redox probes have emerged over the past decades as the preferred tool to measure oxidative stress in vitro due to their easy use, low cost, and non-toxicity [7,8]. Of the different probes available, the fluorogenic 2′,7′-dichlorodihydrofluorescein-diacetate (DCFH$_2$-DA) is amongst the most frequently used redox probes. The acetate groups on DCFH$_2$-DA allow for diffusion across the plasma membrane, after which both groups are cleaved by intracellular esterases to form DCFH$_2$ that is believed to be retained in the cytosol (Figure 1). DCFH$_2$ is reactive towards many types of oxidants, including nitrogen dioxide ($^\bullet NO_2$) [9], the carbonate radical anion ($CO_3^{\bullet -}$) [9], the hydroxyl radical ($^\bullet OH$) [9], Fe^{2+} [10], Cu^+ [10], thiyl radicals (e.g., the glutathione radical; $GS^\bullet$) [11], and peroxidases (e.g., cytochrome c peroxidase) [12]. Following two-electron oxidation, in which superoxide anion ($O_2^{\bullet -}$) is generated as by-product [13], fluorescent DCF is formed that can be visualized or quantified as a nonspecific measure of oxidative stress (Figure 1).
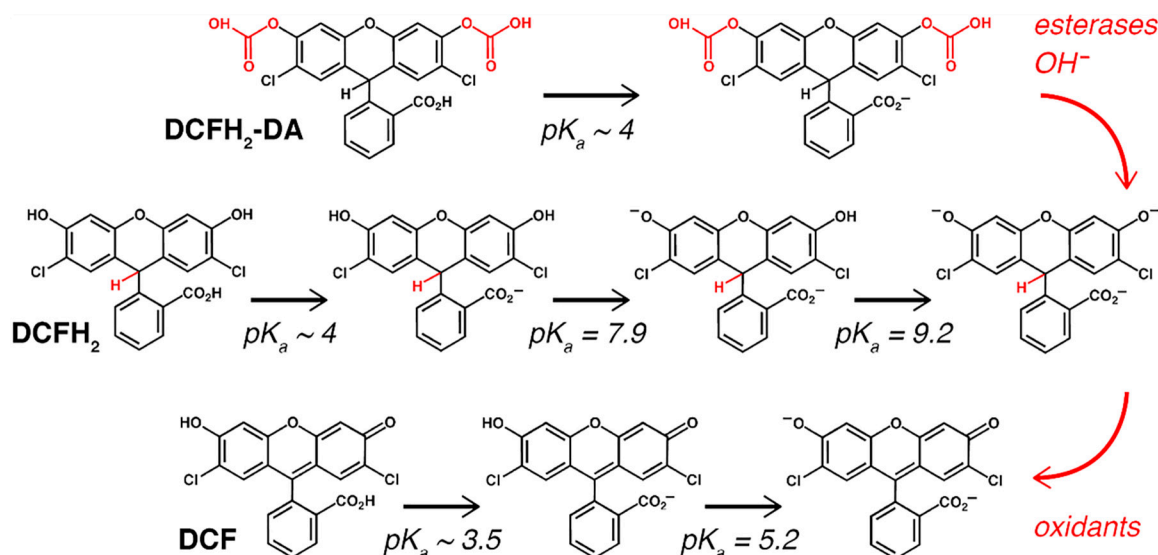

Figure 1. The chemical structure, pH-dependent isoforms, and (estimated) acid dissociation constants (pK$_a$) [14,15] of DCFH$_2$-DA, DCFH$_2$, and DCF. Details are provided in the text.

Despite its widespread application, only limited research has focused on the practical aspects of the in vitro use of DCFH$_2$-DA [16–24]. More specifically, studies on DCFH$_2$-DA uptake, DCFH$_2$ oxidation, and DCF retention in liver cell lines or hepatocytes are lacking. The probe kinetics in vitro are of particular concern given that hepatocytes express a multitude of membrane transporters that have important practical implications for the use of DCFH$_2$-DA [25]. Inasmuch as primary hepatocytes swiftly de-differentiate in monolayer

culture, hepatoma cell lines are commonly employed to study hepatic (patho)physiology in vitro. HepG2 is a human hepatocellular carcinoma-derived cell line that is one of the most widely used cell types for these purposes. The relatively new HepaRG cell line is an increasingly used human hepatocellular carcinoma-derived cell line that has the ability to differentiate over a 4-wk period into a heterogeneous monolayer culture consisting of islets of hepatocyte-like cells that are surrounded by cholangiocyte-like cells [26].

In light of the abovementioned knowledge gaps, this study aimed to optimize the practical applicability of $DCFH_2$-DA in HepG2 cells and undifferentiated (2-wk old) as well as differentiated (4-wk old) HepaRG cells. The most important observations were that extracellular DCF enters HepG2 and HepaRG cells, that DCF is poorly retained in hepatocytes, and that $DCFH_2$ oxidation kinetics in hepatocytes are cell type-specific. Moreover, DCF fluorescence intensity was pH-dependent at pH < 7 and the stability of $DCFH_2$-DA in cell culture medium relied on medium composition. A detailed experimental protocol that corrects for these technical hurdles was developed with the intent to aid researchers in optimizing experimental design and proper analysis of data generated with $DCFH_2$-DA. To further demonstrate the probe's utility under these experimental conditions, $DCFH_2$-DA was used to visualize and quantify oxidative stress in real-time in HepG2 cells subjected to anoxia/reoxygenation.

2. Methods

References to online supplemental material are indicated with prefix 'S.'

2.1. Reagents and Buffers

$DCFH_2$-DA was purchased from Life Technologies/Molecular Probes (Eugene, OR, USA) and dissolved in methanol (MeOH) at a 25-mM stock concentration or in dimethyl-sulfoxide (DMSO) at a 50-mM stock concentration. DCF was acquired from Sigma-Aldrich (St. Louis, MO, USA) and dissolved in DMSO at a 20-mM stock concentration. All other reagents are listed in Table S1. The concentrations listed throughout this manuscript refer to final concentrations unless indicated otherwise.

2.2. Preparation of DCFH2

High-purity $DCFH_2$ was prepared from $DCFH_2$-DA in accordance with an optimized and validated protocol [10]. Briefly, 5 μmol of $DCFH_2$-DA in MeOH was dissolved 2.5 mL of 100 mM NaOH and incubated for 15 min at room temperature (RT) in the dark to ensure complete deacetylation of $DCFH_2$-DA to $DCFH_2$. The solution was subsequently adjusted to pH = 1 by the addition of 2.5 mL of 200 mM HCl to precipitate $DCFH_2$. Next, liquid phase extraction of $DCFH_2$ was performed by the addition of 4 mL of chloroform ($CHCl_3$) to the suspension. After vortexing, the organic phase was aspirated and evaporated under a stream of N_2 gas at RT in the dark. Subsequently, the crystallized $DCFH_2$ was dissolved in MeOH to yield a 92-mM stock solution and stored under N_2 gas at −20 °C.

2.3. Determination of Molar Extinction Coefficients

The molar extinction coefficient (ε) of $DCFH_2$-DA was determined in water, HEPES buffer (10 mM HEPES, 0.88% NaCl, pH = 7.4, 0.292 osmol/kg), and MeOH. $DCFH_2$-DA in DMSO was diluted in the solvent of interest (0–20 μM) and sample absorbance was determined at 258, 259, or 260 nm for water, HEPES buffer, or MeOH, respectively, by UV/VIS absorption spectroscopy (Lambda 18, Perkin Elmer, Waltham, MA, USA) in a 1-cm path length quartz cuvette (Hellma Analytics, Müllheim, Germany). The molar extinction coefficient was subsequently calculated over the complete concentration range in all solvents according to the Beer-Lambert equation [27].

The molar extinction coefficient of $DCFH_2$ in MeOH was recently reported [10]. In addition, the molar extinction coefficient of $DCFH_2$ was determined in water, PBS (pH = 6 or pH = 12), and HEPES buffer (adjusted to pH = 6 or pH = 12 with HCl or NaOH, respectively). $DCFH_2$ in MeOH was prepared in the solvent of interest (0–90 μM) and

sample absorbance was determined at 286 nm for water, PBS (pH = 6), and HEPES buffer (pH = 6), and at 305 nm for PBS and HEPES buffer (both pH = 12).

Similarly, DCF in DMSO was diluted in water (pH = 12), HEPES buffer, MeOH, and DMSO (0–20 μM) and its molar extinction coefficient was calculated at 503 nm, 284 nm, and 535 nm for aqueous solvent (water and HEPES buffer), MeOH, and DMSO, respectively.

2.4. Spectral Properties of $DCFH_2$-DA, $DCFH_2$, and DCF

Concentration-dependent (0–20 μM) ground state absorption spectra were recorded for $DCFH_2$-DA, $DCFH_2$, and DCF in aqueous (MilliQ, HEPES buffer) and organic solvents (MeOH, DMSO).

In addition, pH-dependent absorption spectra of 20 μM DCF and $DCFH_2$ as well as pH-dependent excitation and emission spectra (Cary Eclipse, Varian, Palo Alto, CA, USA) of 20 μM DCF were acquired in unbuffered water adjusted to pH = 1–12 with 37% HCl.

2.5. Stability of $DCFH_2$-DA and $DCFH_2$ in Solvent

The stability of $DCFH_2$-DA and $DCFH_2$ was determined in organic and aqueous solvents. The stability of $DCFH_2$ and $DCFH_2$-DA in MeOH is reported elsewhere [10]. A 20-μM solution of each compound was prepared in DMSO, HEPES buffer, and water. Samples were stored at $-20\ °C$ or $4\ °C$ in the dark and the extent of auto-oxidation (i.e., the formation of DCF) was determined spectrofluorometrically ($\lambda_{ex} = 503 \pm 5$ nm, $\lambda_{em} = 513$–650 nm or $\lambda_{ex} = 535 \pm 5$ nm, $\lambda_{em} = 545$–650 nm for water/HEPES or DMSO, respectively) at different time points over a period of 28 d. The fluorescence emission spectra were integrated and plotted as a percentage of the integrated spectra of a freshly prepared 20-μM DCF sample (reference standard).

The short-term stability of $DCFH_2$-DA was analyzed spectrofluorometrically in PBS and serum-free cell culture media (WE, DMEM, and RPMI-1640) with or without HEPES (25 mM, pH = 7.4) at ambient CO_2 tension. The spectrofluorometer was employed in kinetics mode ($\lambda_{ex} = 500 \pm 5$ nm, $\lambda_{em} = 523 \pm 5$ nm) using continuous magnetic stirring and Peltier-controlled temperature regulation. Solvents/reagents were added to the cuvette in the following order: t = 0 min, 1494 μL of solvent (equilibrated at 37 °C) and t = 1 min, 6 μL of 5 mM $DCFH_2$-DA in DMSO (20 μM final concentration). Fluorescence was recorded over a period of 2 h with continuous acquisition. The fluorescence emission intensity at each time point was plotted as a percentage of the fluorescence emission intensity of a 20-μM DCF reference sample, measured at the end of the kinetics read.

2.6. Cell Culture

HepaRG cells were kindly provided by Biopredic International (Saint-Grégoire, France). HepG2 cells were purchased from ATCC (Manassas, VA, USA). Both cell lines were cultured in WE medium supplemented with 10% (vol/vol) fetal bovine serum, 100 U/mL penicillin, 100 μg/mL streptomycin, 2 mM L-glutamine, 5 μg/mL insulin, and 50 mM hydrocortisone under standard culture conditions (humidified atmosphere of 95% air and 5% CO_2 at 37 °C). Cells were subcultured at a 1:5 ratio (HepG2) or 1:7 ratio (HepaRG) following detachment by trypsinization (15 min at 37 °C) in a 2:1:1 accutase:accumax:PBS mixture. HepG2 cells, undifferentiated HepaRG cells, and differentiated HepaRG cells were used for experiments after 4–5, 12–16, and 26–30 d of culture, respectively. Cells were seeded in 24-wells plates and used at 100% confluence for each experiment.

2.7. Cellular $DCFH_2$-DA Uptake

Time- and concentration-dependent $DCFH_2$-DA uptake were analyzed by incubating cells with 50 μM $DCFH_2$-DA in PBS for 0–20 min or with 0–100 μM $DCFH_2$-DA in PBS for 15 min, respectively. Following incubation, the $DCFH_2$-DA-containing PBS was aspirated, snap frozen in liquid N_2, and stored at $-20\ °C$. At a later time point, samples were thawed and centrifuged for 15 min at $15,000\times g$ (4 °C) to pellet any cellular debris. Next, 400 μL supernatant was incubated with 600 μL of 190 mM NaOH for 15 min at RT in

the dark so as to convert all DCFH$_2$-DA into DCFH$_2$ [10]. The concentration of DCFH$_2$ and DCF (from concurrent auto-oxidation) was determined in each sample by means of absorbance ($\varepsilon_{305\,nm}$ = 7906 M^{-1} · cm^{-1} in PBS, pH = 12) and fluorescence spectroscopy (λ_{ex} = 503 $\pm$ 5 nm, λ_{em} = 513–700 nm against a 0–40-nM DCF standard curve), respectively. The cellular uptake of DCFH$_2$-DA was calculated by subtracting the combined nanomolar amount of DCFH$_2$ and DCF in the supernatant (as a measure of residual DCFH$_2$-DA following incubation) from that of the DCFH$_2$-DA in PBS stock solution (n = 4). Data were subsequently normalized to total protein content per well that was determined in duplicate using a colorimetric commercial kit (bicinchoninic acid [BCA] protein assay, Thermo Scientific, Rockford, IL, USA), as well as to incubation time for the concentration-dependent experiments. The cell lysis solution (0.1 M NaOH and 1% Triton X-100 in water) was chosen because of the different mechanism of cell lysis by NaOH and Triton X-100 and because these components do not interfere in the BCA derivatization reaction and subsequent spectrophotometric determination (described in Section S2.7 and Figures S1 and S2).

2.8. Cellular DCF Uptake

To investigate time-dependent uptake of DCF, cells were incubated with 50 µM DCF in serum-free WE medium for 0–20 min under standard culture conditions. At each time point, cells were washed twice with PBS and lysed with lysis solution (250 µL/well) for 1 h at 37 °C. Following homogenization of cell lysates by rocking, DCF fluorescence was measured using a microplate reader (λ_{ex} = 460 $\pm$ 40 nm and λ_{em} = 520 $\pm$ 20 nm; BioTek Instruments, Winooski, VT, USA). Data were corrected for total protein content per well as described above and normalized to controls (i.e., 0 min incubation).

Concentration-dependent DCF uptake was determined by incubating cells with 0–100 µM DCF in serum-free WE medium for 20 min under standard culture conditions. Subsequently, cells were washed twice in PBS and 300 µL of PBS was added to each well. DCF fluorescence was measured at abovementioned settings, corrected for total protein content per well as well as for incubation time, and normalized to control (i.e., 0 µM DCF).

2.9. Intracellular DCF Retention and Transmembrane Diffusion

The extent of intracellular DCF retention was determined by incubating cells in serum-free WE medium with 100 µM DCF or solvent control for 2 h at standard culture conditions. Cells were washed twice in PBS and 500 µL of serum-free WE medium was added to each well, which was aspirated at various time points over a 20-min period. Next, cells were lysed and DCF fluorescence in the lysate was determined as described above.

Intracellular DCF retention was also visualized by laser-scanning confocal microscopy (Leica SP8, Leica Microsystems, Wetzlar, Germany). HepG2 cells were grown to confluence in 6-well plates pre-coated with rat tail-derived collagen I in 0.1 M acetic acid in water for 6 h (8 µg/cm^2). Prior to imaging, cells were incubated with 100 µM DCF in serum-free WE medium for 2 h at standard culture conditions. Thereafter, cells were washed twice with PBS and fixed in 1.5 mL of fixative (4% paraformaldehyde and 2% sucrose in PBS, 5 min, RT) following 5- or 30-min incubation with serum-free WE medium. Cells were stained with 1 µM Nile Red in PBS (from 5 mM Nile Red in DMSO stock solution) for 60 s and washed thrice with 1 mL of PBS [28,29]. The coverslips were then mounted on microscope slides using DAPI-containing Vectashield mounting medium (Vector Laboratories, Burlingame, CA, USA). Fluorescence intensity was measured per fluorophore at λ_{ex} = 405 nm, λ_{em} = 415–480 nm for DAPI; λ_{ex} = 540 nm, λ_{em} = 550–650 nm for Nile Red; and λ_{ex} = 495 nm, λ_{em} = 520–580 nm for DCF. An overlay image was composed of the individually acquired images. Laser and detector settings were kept constant throughout the experiment.

The transmembrane diffusibility of DCF was assessed using liposomes encapsulating DCF or 6-carboxyfluorescein (CF) at a self-quenching concentration. CF (49 mM) and DCF (18 mM) were prepared in 98.4 and 37.3 mM NaOH in water, respectively, and incubated overnight at 37 °C under continuous shaking. Both solutions were gradually titrated to

pH = 7.4 with 37% HCl under continuous magnetic stirring, after which solvent osmolarity was determined as described in [30] against a 0–154-mM NaCl in water (pH = 7.4) standard curve and adjusted to 0.292 osmol/kg with NaCl. Liposomes were prepared by the lipid film hydration technique as described in [10]. Briefly, a lipid film was prepared by mixing stock solutions of DMPC, cholesterol, lactosyl-PE, and GM1 at a 50:40:5:5 molar ratio (10 mM final lipid concentration). The solvent was evaporated under a stream of N_2 gas followed by 30 min of vacuum desiccation. The resulting lipid film was hydrated with 500 µL of self-quenching DCF or CF solution and sonicated using a tip sonicator (Branson Ultrasonics, Danbury, CT, USA) for 5 min. Unencapsulated probe was subsequently removed by size exclusion chromatography according to [31].

The release of encapsulated DCF or CF was determined over a period of 10 min by fluorescence spectroscopy (λ_{ex} = 491 $\pm$ 5 nm, λ_{em} = 523 $\pm$ 5 nm). A cuvette containing 1500 µL of HEPES buffer was placed into the spectrometer (maintained at 22 °C) and time-based acquisition was started. At t = 1 min, 40 µL of iso-osmotic liposome solution was added. At t = 9 min, 15 µL of 15% TX-100 in water was added to lyse the liposomes, resulting in the release of all encapsulated probe and hence maximum fluorescence intensity.

2.10. Basal Oxidant Formation and Cellular Metabolic Rate

To analyze the intracellular basal oxidant formation, cells were incubated with 0–100 µM DCFH$_2$-DA in serum-free HEPES-buffered WE medium (25 mM, pH = 7.4) at 37 °C in a microplate reader in which DCF fluorescence was measured over a period of 2 h at 10-min intervals (λ_{ex} = 460 $\pm$ 40 nm, λ_{em} = 520 $\pm$ 20 nm). A cell-free plate was analyzed directly thereafter to determine the rate of DCFH$_2$-DA auto-oxidation in the incubation medium. Cellular DCF fluorescence was adjusted for DCFH$_2$-DA auto-oxidation over time and normalized to total protein content per well.

Cellular O_2 consumption and extracellular acidification rate (ΔpH) were determined as a measure for the overall metabolic rate in cells seeded onto 96-well plates (Seahorse Bioscience, North Billerica, MA, USA). Cells were analyzed in 200 µL serum- and bicarbonate-free DMEM using a Seahorse XF96 analyzer (Seahorse Bioscience; n = 24 per cell type, 3 measurements per sample). All data were normalized to total protein content per well.

2.11. Real-Time Analysis of Oxidant Formation during In Vitro Anoxia/Reoxygenation in HepG2 Cells

DCFH$_2$-DA was used to visualize acute oxidative stress in HepG2 cells under experimental conditions emulating hepatic ischemia-reperfusion [32]. For this purpose, a custom-built fluorescence microscopy-based experimental setup was used (Figure S3). HepG2 cells were cultured on collagen-coated (as described above) 0.8-mm channel slides (Ibidi, Planegg, Germany).

During the experiment, cells were perfused (80 µL/min) with serum-, glucose-, and pyruvate-free WE medium for 4 h at 37 °C. The medium was continuously purged with a mixture of 95% N_2 and 5% CO_2 or 95% air and 5% CO_2 (Linde Gas Benelux, Schiedam, The Netherlands) for the anoxia-reoxygenation (A/R) or control group, respectively. The slide was subsequently perfused with 100 µM DCFH$_2$-DA in the respective incubation medium for 15 min (80 µL/min). In an additional A/R intervention group, 1 mM dimethyl malonate (DMM), which prevents the build-up of succinate during anoxia and hence reduces oxidant formation upon reoxygenation [33], was added to the perfusion medium and the DCFH$_2$-DA-containing incubation medium.

Following incubation with DCFH$_2$-DA, perfusion was resumed with medium purged with 95% O_2 and 5% CO_2 in the A/R and A/R intervention groups. Cells in the control group were perfused with medium saturated with 95% air and 5% CO_2. Immediately after wash-out of the DCFH$_2$-DA incubation medium (~10 s), cells were visualized with a stereo fluorescence microscope (λ_{ex} = 470 $\pm$ 20 nm, λ_{em} = 515 nm long pass; model M165 C, Leica Microsystems, Wetzlar, Germany) for a period of 30 min at 2.5-min intervals with dark intermittence periods. Cellular DCF fluorescence was subsequently quantified based on

total pixel intensity of the images following conversion to 8-bit grayscale (ImageJ software; National Institutes of Health, Bethesda, MD, USA) and normalized to t = 0 min.

2.12. Statistical Analysis

Statistical analysis was performed using GraphPad Prism (GraphPad Software, La Jolla, CA, USA). All data were analyzed using one-way ANOVA, in which repeated-measures data were analyzed based on area under the curve (AUC) values per sample. Intragroup multiple comparisons were made using the Dunnet's post-hoc test, where means were compared to a single control. For intergroup multiple comparisons, all possible pairs of means were compared using Tukey's range test. A *p*-value of < 0.05 was considered statistically significant.

3. Results

3.1. The Spectral Properties of $DCFH_2$-DA and Derivatives Are pH-Dependent

The spectral properties of $DCFH_2$-DA, $DCFH_2$, and DCF were analyzed using absorbance and fluorescence spectroscopy, the results and discussion of which are provided in Section S3.1 and Figures S4–S6. The most important and relevant finding was that changes in pH (up to pH = 8.0) affect the absorption spectrum and fluorescence emission and excitation spectra of DCF. Therefore, changes in pH are likely to affect experimental data interpretation and outcomes, particularly under conditions of acidosis.

3.2. The Stability of $DCFH_2$-DA and $DCFH_2$ in Aqueous Solvent and Medium Is Dependent on the Composition of the Solution

The long- and short-term stability of $DCFH_2$-DA and $DCFH_2$ was analyzed in aqueous solvents (discussed in the Supplemental Information) and cell culture media (the latter only for $DCFH_2$-DA). Decay of $DCFH_2$-DA in aqueous solution, resulting in the formation of DCF, most likely occurs through base-catalyzed hydrolysis of the acetate groups and subsequent $DCFH_2$ (auto-)oxidation. DCF generation as a measure for $DCFH_2$-DA decay was analyzed spectrofluorometrically in solutions containing 20 μM $DCFH_2$-DA and plotted as percentage of a 20-μM DCF reference sample (Figure 2).

Temperature- and solute-related effects were observed when the short-term stability of $DCFH_2$-DA was determined in different types of cell culture media (WE, DMEM, and RPMI-1640) and PBS; conditions that are relevant for in vitro use of the probe. DCF formation in PBS was undetectable at RT and negligible at 37 °C following 2 h of incubation (Figure 2A), which is in line with the data on long-term stability of $DCFH_2$-DA in aqueous solvent (Figure S7). $DCFH_2$-DA stability in cell culture medium (37 °C) was analyzed at ambient CO_2 tension in serum- and phenol red-free DMEM, RPMI, and WE with or without HEPES (25 mM, pH = 7.4). The reason for this was that microplate-based experiments involving $DCFH_2$-DA (as described below) generally need to be performed under these conditions. Considerable variation in the extent of DCF formation was noted for the different types of culture medium and depending on the presence of HEPES. Given that HEPES prevents medium alkalization at ambient CO_2 tension, its presence was expected to improve $DCFH_2$-DA stability due to a reduction in $[OH^-]$-mediated deacetylation. However, addition of HEPES to the different medium formulations resulted in opposing effects on DCF formation. Specifically, the presence of HEPES deterred DCF formation in WE (Figure 2B), favored it in DMEM (Figure 2C), and had no noticeable effect in RPMI (Figure 2D). Considering that the influence of HEPES on DCF formation appears to be independent of its presumed inhibitory effect on $DCFH_2$-DA deacetylation, the observed differences most likely result from complex interactions between $DCFH_2$, HEPES, and redox-active medium components (Table 1). In that regard, the extent of DCF formation in DMEM corresponds well to it being the most nutrient-rich medium with a high concentration of $O_2^{\bullet-}$-producing riboflavin, granted that (room) light is present to facilitate this reaction [34]. DMEM is moreover the only medium containing Fe^{3+} that, together with $O_2^{\bullet-}$, will result in the formation of redox-active Fe^{2+} through Haber-Weiss cycling [35].
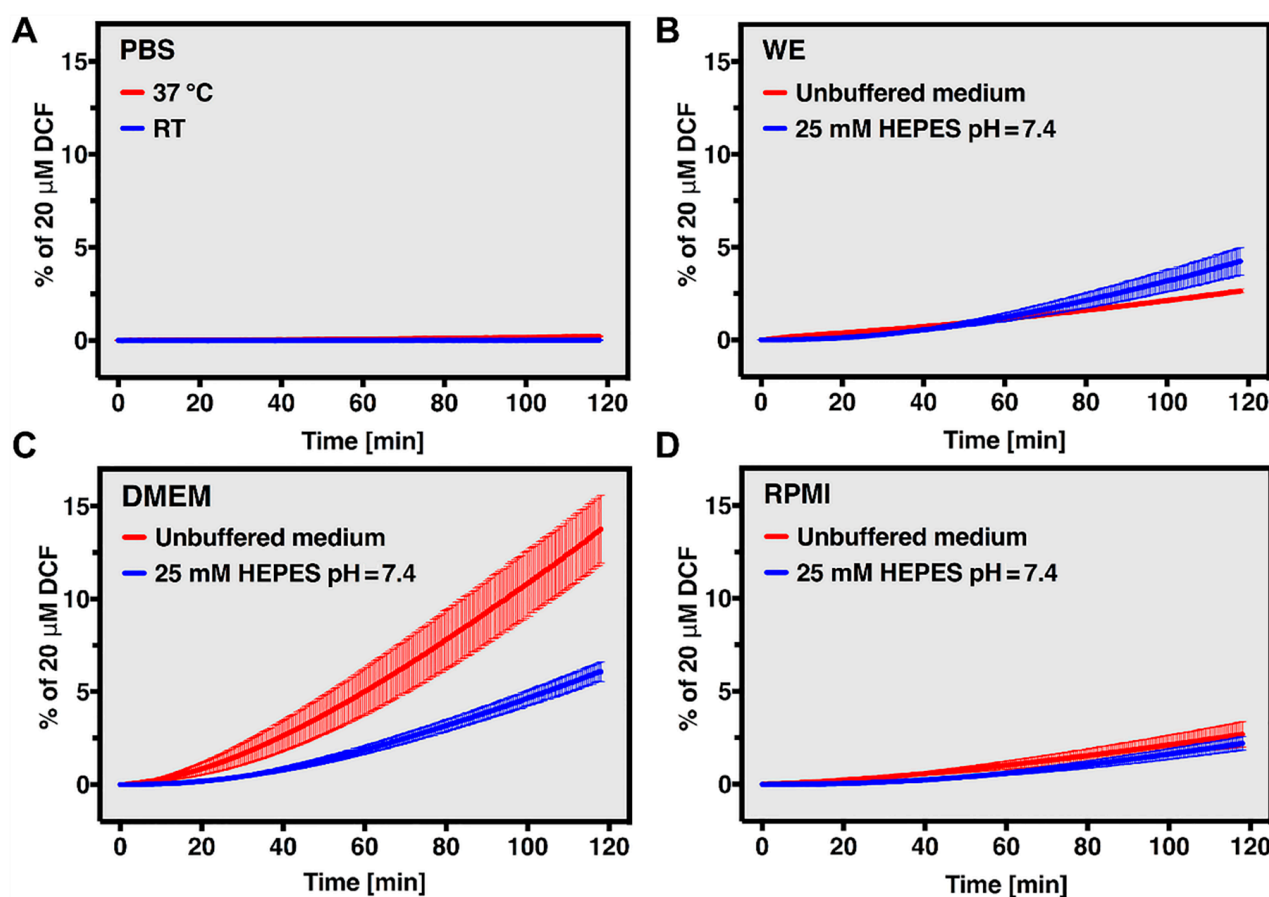
Figure 2. Stability of DCFH$_2$-DA in PBS and medium. (**A**) Stability of 20 μM DCFH$_2$-DA in PBS measured at room temperature (RT; blue line) or 37 °C (red line) over a period of 2 h. DCFH$_2$-(DA) stability was measured by means of DCF formation and plotted as a percentage of a 20-μM DCF reference sample. (**B**–**D**) Stability of 20 μM DCFH$_2$-DA in (**B**) unbuffered (red line) and HEPES-buffered (25 mM, pH = 7.4; blue line) William's E (WE), (**C**) Dulbecco's modified Eagle medium (DMEM), and (**D**) Roswell Park Memorial Institute (RPMI) medium measured at 37 °C over a period of 2 h. DCFH$_2$-(DA) stability was measured by means of DCF formation and plotted as a percentage of a 20-μM DCF reference sample. All data (n = 3/group) are plotted as mean ± SD.

Table 1. Redox-active compounds in common cell culture media. All compounds are listed in μM concentration, calculated from the manufacturer's data sheets (Table S1).

		DMEM	**RPMI**	**WE**
Salts	Fe^{3+} (nitrate)	0.25	0.00	0.00
Vitamins	Ascorbic acid	0.00	0.00	11.36
	Riboflavin	1.06	0.53	0.27
Amino acids	Cysteine	0.00	0.00	330.17
	Histidine	270.69	96.67	96.67
	Methionine	201.06	100.53	100.53
	Phenylalanine	399.54	90.80	151.34
	Tryptophan	78.34	24.48	48.96
	Tyrosine	397.37	110.38	193.17
Other compounds	GSH	0.00	3.25	0.16

Although all types of media contain varying amounts of antioxidants (e.g., GSH and ascorbic acid), these radical-scavenging compounds become radicals themselves upon oxidation [7]. Hence, 'antioxidants' can also function as pro-oxidants under the appropriate circumstances. Accordingly, the free radical scavengers GSH [36], cysteine [36], and

ascorbic acid [37] were all shown to generate H_2O_2 in DMEM and/or RPMI. Addition of another compound with similar properties, in this case HEPES [38,39], could therefore shift the redox equilibrium of the sample in opposing ways. As a result, the extent to which $DCFH_2$ oxidation takes place will strongly depend on medium composition. The addition of HEPES to WE, for instance, could result in HEPES reacting with ascorbic acid radicals (formed as a result of, e.g., $O_2^{\bullet-}$ generation by riboflavin [40,41]) that would otherwise be converted into redox-unreactive dehydroascorbic acid. Consequently, HEPES would function as a catalyst for $O_2^{\bullet-}$ formation [38] and thereby enhance $DCFH_2$ oxidation (Figure 2B). In DMEM, which contains a large portion of oxidant-generating compounds together with low levels of antioxidants, HEPES will likely act as a free-radical sink, consequently reducing the formation of DCF (Figure 2C).

In conclusion, although $DCFH_2$-DA is relatively stable in aqueous solution when kept at 4 °C for up to 24 h, long-term storage in water or physiological buffers is not recommended. It is also advisable to take the effects of cell culture media components into consideration when performing in vitro assays using $DCFH_2$-DA, and preferably not use DMEM.

3.3. $DCFH_2$-DA Rapidly Accumulates in HepG2 and HepaRG Cells

Uptake of $DCFH_2$-DA as a function of time and concentration was analyzed in HepG2 and undifferentiated as well as differentiated HepaRG cells (Figure 3). Time-dependent uptake of $DCFH_2$-DA was rapid, as evinced by the presence of detectable amounts of $DCFH_2$-DA at t = 0 min (i.e., very brief contact between the monolayer and the incubation medium), and plateaued at t = 5 min in all groups (Figure 3A). These data indicate that a $DCFH_2$-DA incubation time of 5–10 min suffices for single-read experiments. The findings are consistent with reports on the uptake of $DCFH_2$-DA by Chinese hamster ovary cells [16] and on the hepatocellular uptake of 5(6)-carboxy-2'7'-dichlorofluorescein diacetate (carboxy-DCF-DA) [42]. Passive diffusion is generally assumed to be the main uptake mechanism for $DCFH_2$-DA [43], as was demonstrated by linear uptake of carboxy-DCF-DA (measured intracellularly through its deacetylation product carboxy-DCF) over a 0–500-μM range [42]. In contrast, the $DCFH_2$-DA uptake rate in HepG2 and HepaRG cells deviated from linearity at 100 μM (Figure 3B–D), which might indicate a greater role for uptake through plasma membrane transporters such as organic anion transporting proteins 1B1 and 1B3 (OATP1B1 and OATP1B3, respectively) [44]. However, saturation of hepatocellular carboxy-DCF uptake, which strongly depended on OATP activity, did not occur until concentrations exceeded 100 μM [42]. Finally, the intracellular accumulation of carboxy-DCF was significantly decreased at 4 °C compared to 37 °C incubation (at 4 °C the rate of endocytosis and enzymatic/transporter activity is vastly reduced), whereas uptake of its acetylated derivate was temperature-independent [42]. Accordingly, transporter-mediated $DCFH_2$-DA uptake is likely not a major contributor to probe accumulation.

Saturation of cytosolic esterase activity could form an alternative explanation for the observed plateau in the $DCFH_2$-DA uptake rate. Assuming that cellular $DCFH_2$-DA uptake mainly proceeds through passive diffusion, intracellular [$DCFH_2$-DA] will not exceed extracellular [$DCFH_2$-DA], i.e., that in the incubation medium. The concomitant esterase-dependent intracellular formation of $DCFH_2$ however establishes a $DCFH_2$-DA sink that allows for ongoing probe influx. Thus, when this enzymatic process becomes saturated, the concentration gap between intracellular and extracellular [$DCFH_2$-DA] will stabilize as a result of which probe uptake will concomitantly not increase at higher probe concentrations. This principle has been shown for acetylsalicylate uptake by hepatocytes co-incubated with the acetylesterase inhibitor paraoxon [45]. The presumed acetylesterase-dependency of $DCFH_2$-DA uptake could further explain the differences in uptake rate between, e.g., HepG2 and differentiated HepaRG cells (Figure 3B,D), and underscores the notion that $DCFH_2$-DA accumulation is likely cell-type specific.
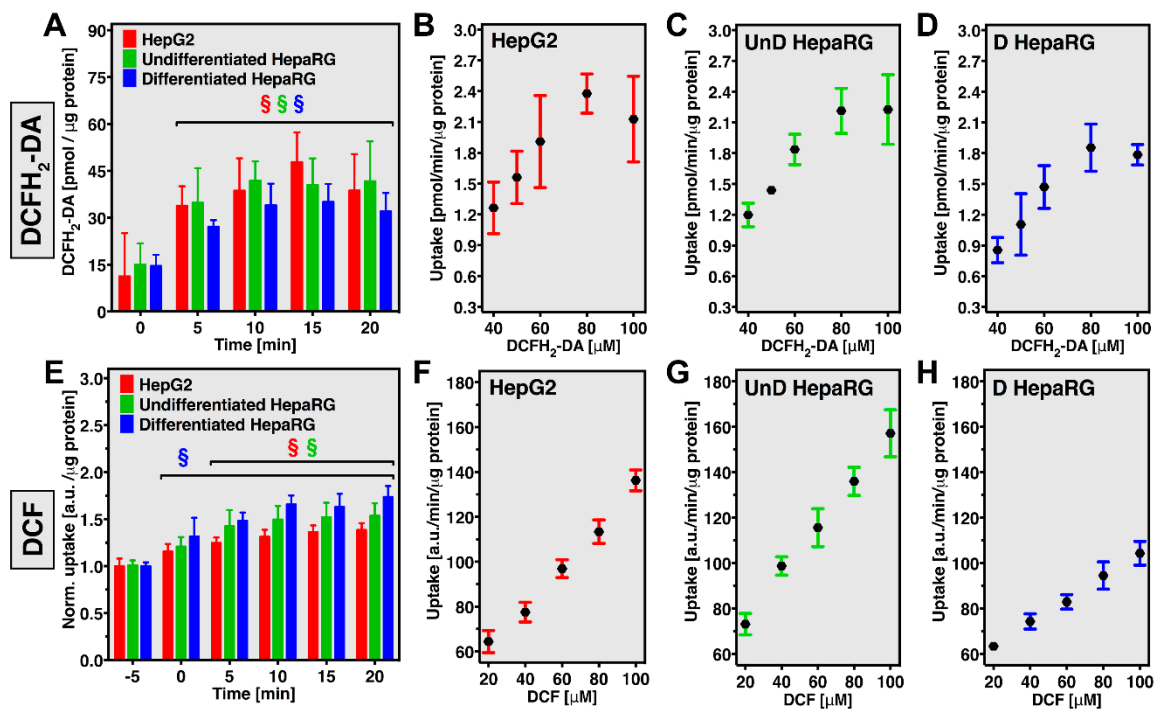
Figure 3. Time-dependent uptake and cellular uptake rates of $DCFH_2$-DA and $DCFH_2$ by HepG2 and HepaRG cells. (**A**) Time-dependent uptake of 50 μM $DCFH_2$-DA (pmol/μg protein) by HepG2 (red bars), undifferentiated (green bars), and differentiated HepaRG cells (blue bars). $DCFH_2$-DA uptake rates (pmol/min/μg protein) for (**B**) HepG2, (**C**) undifferentiated, and (**D**) differentiated HepaRG cells, determined for 40–100 μM $DCFH_2$-DA. (**E**) Time-dependent uptake of 50 μM DCF (a.u./μg protein) by HepG2 (red bars), undifferentiated (green bars), and differentiated HepaRG cells (blue bars). DCF uptake rates (a.u./min/μg protein) for (**F**) HepG2, (**G**) undifferentiated, and (**H**) differentiated HepaRG cells, determined for 20–100 μM DCF. All data (n = 8/group) are plotted as mean ± SD. Statistical significance ($p < 0.05$) is designated '§' for intragroup analyses.

3.4. DCF Accumulates in HepG2 and HepaRG Cells and Is Poorly Retained

The cellular uptake and excretion of DCF were analyzed because such effects are expected to skew experimental data in an upward or downward direction, respectively, when using $DCFH_2$-DA to assay intracellular oxidative stress. DCF uptake was determined in a time- and concentration-dependent manner. The fluorophore accumulated swiftly in all cell types, yet more rapidly in differentiated HepaRG cells compared to HepG2 and undifferentiated HepaRG cells (Figure 3E), as evidenced by significant accumulation at t = 0 min in differentiated HepaRG cells compared to t = 5 min in HepG2 and undifferentiated HepaRG cells. Accordingly, overall DCF uptake was higher in differentiated HepaRG cells ($p < 0.0001$ and 0.001 compared to HepG2 and undifferentiated HepaRG cells, respectively, at t = 20 min) as well as in undifferentiated HepaRG compared to HepG2 cells ($p < 0.01$ at t = 20 min). This trend roughly corresponds to RNA expression levels of OATP1B1 and OATP1B3 that followed differentiated HepaRG > undifferentiated HepaRG >> HepG2 cells [44]. Insofar as culture conditions for differentiated HepaRG cells differed between the referenced study and this study, these results might not be fully superimposable. Considering that OATP1B1 and OATP1B3 are involved in the hepatocellular uptake of carboxy-DCF [42] as well as fluorescein [25,46], both are likely to transport DCF as well. Although DCF is generally assumed to be membrane-impermeable, uptake through passive diffusion could also take place (as discussed below). These findings are of particular relevance for experiments in which prolonged incubation with $DCFH_2$-DA is desired because considerable DCF formation from $DCFH_2$-DA decay occurs under such conditions (Section 3.2, Figure 2).

The DCF uptake rate was linear over the complete concentration range in all cell types (Figure 3F–H), in accordance with data on carboxy-DCF showing that saturation

occurs at [DCF] > 100 μM [42]. In contrast to time-dependent DCF uptake (Figure 3E), the DCF uptake rate was lower in differentiated HepaRG cells compared to HepG2 and undifferentiated HepaRG cells. Time-dependent DCF uptake was measured in cell lysates, whilst the DCF uptake rate was analyzed in intact monolayer culture. This difference in experimental setup opens up the possibility that the overall probe distribution over the complete sample (i.e., cells and incubation medium) may differ, which might affect DCF fluorescence emission properties. Nevertheless, the data collectively show that DCF formation in the incubation medium could interfere with intracellular measurements and that the extent of this effect is cell-type specific.

Intracellular DCF retention was quantified spectrofluormetrically and visualized using confocal microscopy. A rapid reduction in DCF fluorescence, i.e., probe efflux, was observed for all cell types. DCF efflux stabilized at t = 20 min, at which point ~50% of initial probe fluorescence was detected (Figure 4A). DCF expulsion occurred more rapidly in differentiated HepaRG cells compared to HepG2 cells ($p < 0.001$ at t = 5 min) and undifferentiated HepaRG cells ($p < 0.001$ at t = 10 min). As for DCF uptake and OATP1B1/3, this trend fits well with RNA expression levels of the basolateral exporter multidrug resistance protein 3 (MRP3) that followed differentiated HepaRG > undifferentiated HepaRG >> HepG2 cells [44], although differences in culture medium composition for the differentiated HepaRG cells need to be taken into consideration. Although both MRP3 and the apically located MRP2 expel carboxy-DCF from hepatocytes in vivo [42], MRP2 likely does not contribute to DCF efflux in monolayer culture because of its cytosolic localization under these conditions [47]. Correspondingly, MRP2 mRNA expression levels were comparable between all cell types [44].

Efflux of DCF into the extracellular space was confirmed using confocal microscopy of HepG2 cells that were loaded with 100 μM DCF prior to imaging at t = 5 and 30 min following replacement of the incubation solution with probe-free WE medium (Figure 4B,C, respectively). At t = 5 min, DCF was already localized both intracellularly and in the extracellular spaces (indicated by white arrows in Figure 4B, overlay panel). The co-localization between DCF and Nile Red indicates that DCF accumulates in organelles. Considering that the hepatic metabolism of fluorescein proceeds through glucuronidation [48], it is plausible that DCF is processed similarly and therefore localizes in the endoplasmic reticulum. Significant loss of intracellular and extracellular DCF fluorescence was observed at t = 30 compared to t = 5 min, supporting the notion that DCF is actively excreted by HepG2 cells. Glucuronidation of DCF might additionally contribute to the observed loss in fluorescence since the fluorescence intensity of glucuronidated fluorescein constitutes only 4.5% of that of unconjugated fluorescein [48], although further work is needed to substantiate this.

In conclusion, DCF uptake and efflux both occur in HepG2 and HepaRG cells, presumably through transporter-mediated mechanisms. Movement of DCF across the plasma membrane needs to be taken into account when performing assays involving DCFH$_2$-DA on these cell types, as it is expected to affect experimental outcomes.

3.5. DCF Crosses Membranes

The membrane-crossing ability of DCF was investigated by means of liposomes encapsulating DCF and the more hydrophilic 6-carboxyfluorescein (CF) at self-quenching concentrations, a system that generates fluorescence upon probe leakage [31]. An increase in fluorescence (i.e., probe efflux) was observed directly after the addition of DCF-encapsulating liposomes to the iso-osmotic buffer solution, something that was not observed for CF-encapsulating liposomes (Figure 4C). CF differs from DCF in that it lacks the two chlorine moieties but has an additional carboxylic acid group, giving it an overall charge of −3 at physiological pH [49] compared to −2 for DCF (Figure S8 and Figure 1) [14]. It is likely that this difference in charge explains the passage of DCF, but not CF, across the negatively charged phospholipid bilayer that normally deters the diffusion of negatively charged small molecules [50]. Despite providing information on the ability of DCF to cross phospholipid membrane, the experimental setup employed here greatly differs from in vitro

conditions. Most relevantly, the high intraliposomal DCF concentration (18 mM) creates a nonphysiological but significant concentration gradient that potentially favors DCF efflux even at iso-osmotic conditions.
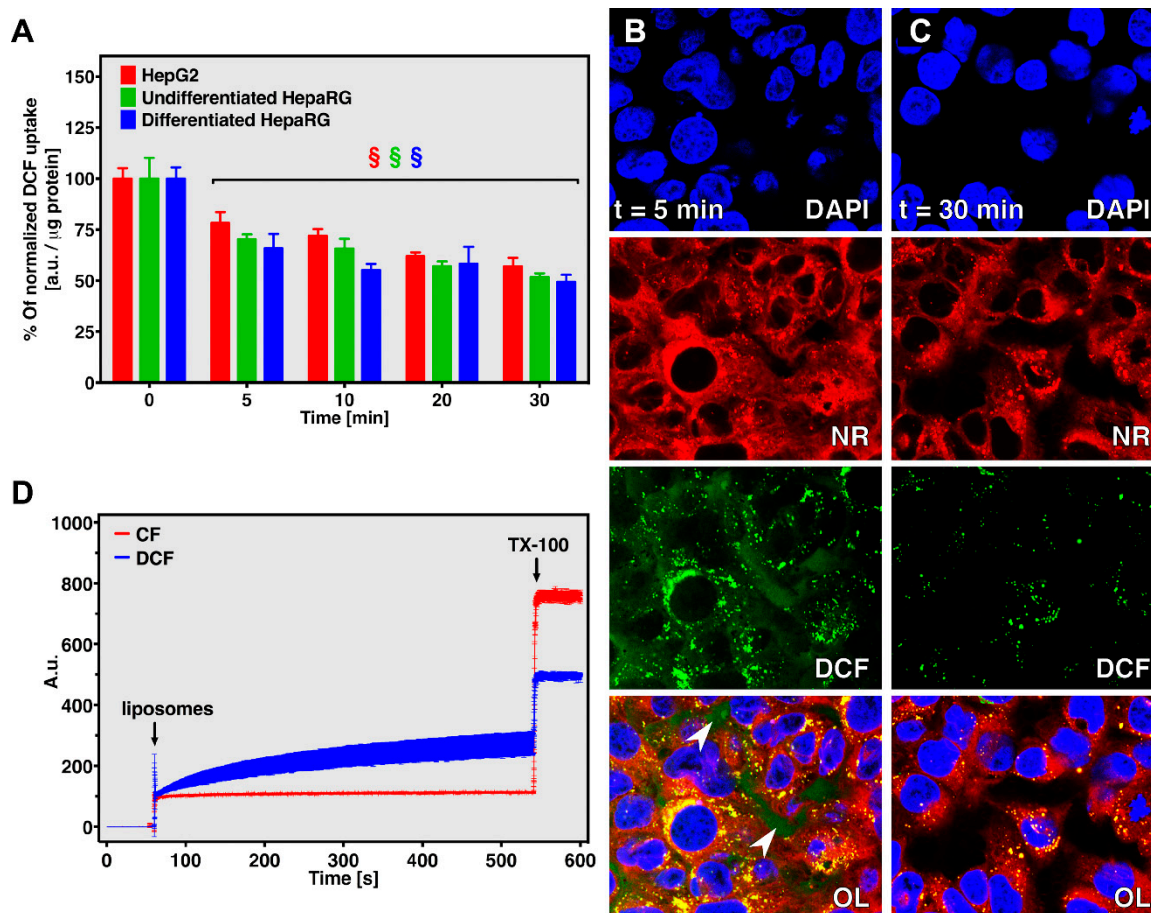

Figure 4. DCF retention in cells and liposomes. (**A**) DCF retention (a.u./µg protein) was measured in HepG2 (red bars), undifferentiated HepaRG cells (green bars), and differentiated HepaRG cells (blue bars) loaded with 100 µM DCF for 2 h. Data (n = 8/group) are plotted as mean ± SD. Intragroup statistical differences ($p < 0.05$) are designated with '§'. (**B**,**C**) Intracellular and extracellular localization of DCF in HepG2 cells loaded with 100 µM DCF for 2 h following (**B**) t = 5 min and (**C**) t = 30 min of incubation in probe-free medium. Cells were counterstained with DAPI (nucleus) and Nile Red (NR; membranes). OL: overlay. The arrowheads in (**B**, overlay) point to the extracellular presence of DCF. (**D**) Efflux of DCF (blue line) and CF (red line) from liposomes encapsulating the probes at self-quenching concentration was analyzed spectrofluorometrically ($\lambda_{ex} = 491 \pm 5$ nm and $\lambda_{em} = 523 \pm 5$ nm) in time-based acquisition mode (t = 600 sec) at 37 °C. At t = 550 s, 0.15% Triton X-100 (TX-100) was added to disrupt the liposomal membrane and release all encapsulated probe. Data (n = 3) are plotted as mean ± SD.

3.6. Basal Oxidant Formation and Cellular Metabolic Rate Differ between HepG2 and HepaRG Cells

The rate of basal oxidant production over time was analyzed at increasing concentrations of DCFH$_2$-DA in HepG2 and undifferentiated as well as differentiated HepaRG cells to ascertain the optimal probe concentration for assays involving these cell types. DCF formation (as a measure for intracellular oxidant formation) correlated to DCFH$_2$-DA concentration up to 60 µM in all cell types (Figure 5A–C), indicating that intracellular probe levels likely reach saturating conditions at $\geq$ 60 µM in resting cells. Overall, DCF formation was significantly higher in HepG2 cells compared to undifferentiated and differentiated HepaRG cells ($p < 0.001$ following 2 h incubation at 80 µM for both groups), likely due to a more pro-oxidant redox state in HepG2 cells. This notion is supported by

the data on cellular O_2 consumption and extracellular acidification rate, which suggest a higher metabolic rate, more glycolytic state, and/or differences in uncoupling processes in HepG2 cells compared to both types of HepaRG cells (Figure 5D,E; $p < 0.001$ for both groups). Accordingly, glucose consumption and lactate production are higher in HepG2 cells compared to (differentiated) HepaRG cells [51]. Nevertheless, the difference in DCF formation between HepG2 and HepaRG cells could also, in part, derive from variations in DCF metabolism that can affect DCF fluorescence intensity as described above. Antioxidant chemotypes could further differ between the cell lines and in this way lead to a difference in DCF formation. Gene expression for common antioxidant proteins did not greatly differ between the cell lines, with the exception of peroxiredoxin-6 and catalase, which were in the order of differentiated and undifferentiated HepaRG > HepG2 cells [44]. Overall, the extent of basal oxidant formation in resting HepG2 and HepaRG cells roughly correlates to lactate formation and O_2 consumption and is best measured at a $DCFH_2$-DA concentration of ≥ 60 μM.
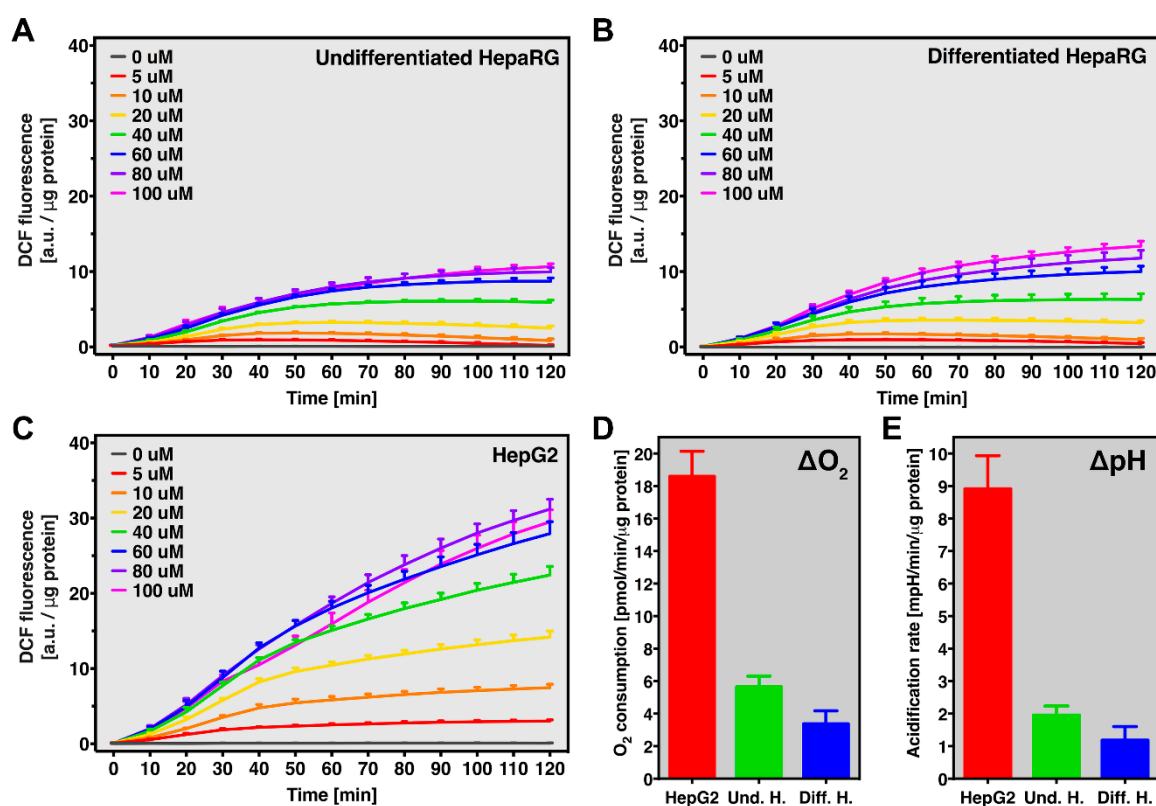
Figure 5. Basal oxidant formation and cellular metabolic rate in HepG2 and HepaRG cells. DCF fluorescence (a.u./μg protein) over time at increasing $DCFH_2$-DA concentration (0–100 μM) as a measure of basal oxidant formation in (**A**) resting undifferentiated HepaRG, (**B**) differentiated HepaRG cells, and (**C**) HepG2 cells. Data (n = 6/group) are presented as mean ± SD. (**D**) Cellular O_2 consumption (pmol/min/μg protein) and (**E**) extracellular acidification rates (mpH/min/μg protein) of HepG2 (red bars), undifferentiated HepaRG cells (Und. H.; green bars), and differentiated HepaRG cells (Diff. H.; blue bars). Data (n = 8/group) are presented as mean ± SD.

3.7. Oxidative Stress during In Vitro Anoxia/Reoxygenation Can Be Visualized in Real-Time Using DCFH_2-DA

$DCFH_2$-DA was used to visualize and quantify acute oxidative stress in HepG2 cells subjected to 4 h of anoxia followed by reoxygenation (A/R) in a perfusion setup equilibrated to 37 °C and positioned under a fluorescence microscope (Figures 6A and S3). Control cells were exposed to standard culture conditions, i.e., medium saturated with 95% air and 5% CO_2, throughout the experiment. A rapid and significant increase in DCF fluorescence was observed in the cells subjected to A/R (Figure 6B,C). DCF fluorescence

intensity reached a maximum at 10–12 min of reoxygenation and subsequently declined, presumably due to a reduced rate of DCF formation at constant DCF efflux and possibly due to metabolism. Considering that hepatocytes exposed to anoxia become acidic [52], the observed increase in DCF formation in this early phase of reoxygenation could well be underestimated due to reduced DCF fluorescence emission at pH < 7 (Figure S6D). In comparison, a decrease in DCF fluorescence was observed in control cells following incubation with DCFH$_2$-DA despite higher fluorescence at baseline (Figure 6C,E). This phenomenon is attributable to the difference in incubation conditions between the control and A/R group, i.e., oxygenated vs. deoxygenated medium, which enabled DCFH$_2$ oxidation to take place in control cells but not in A/R cells during the incubation period.
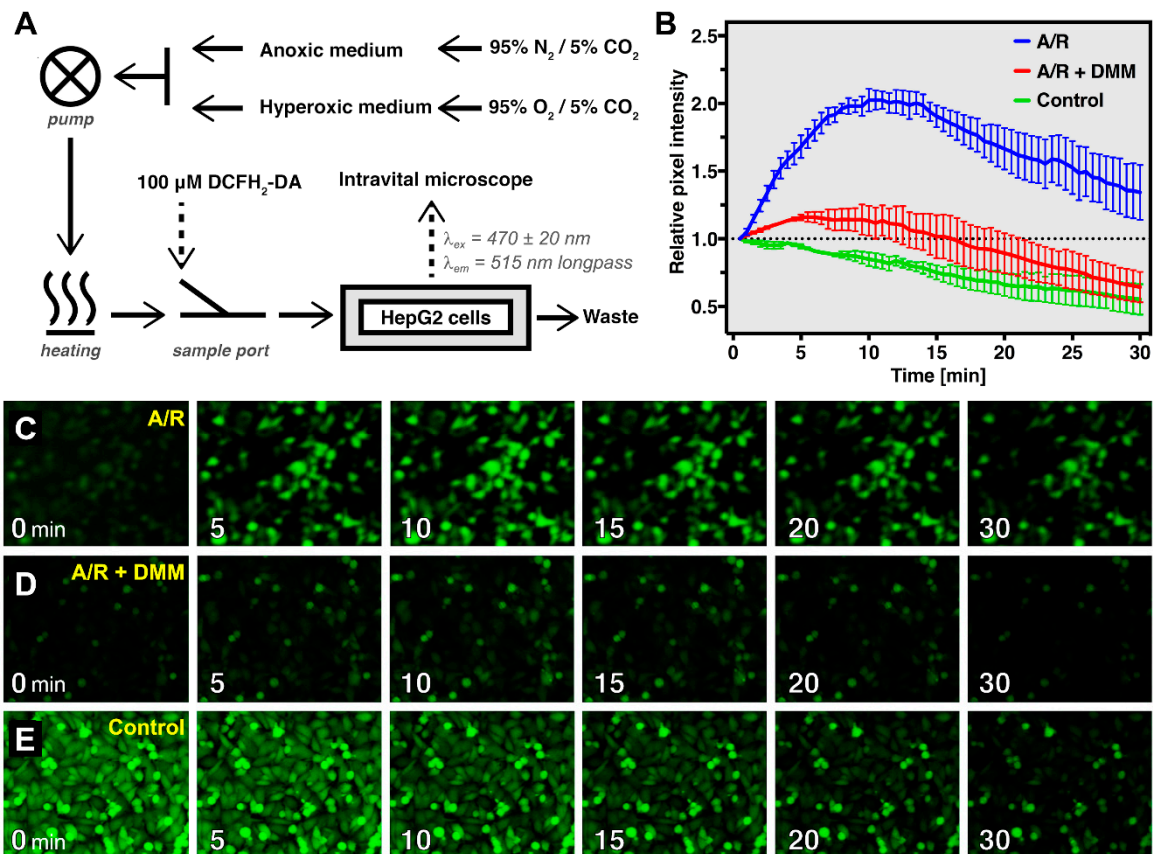
Figure 6. Real-time visualization of oxidative stress during in vitro anoxia-reoxygenation (A/R). (**A**) Schematic overview of the perfusion setup under conditions of A/R; details are provided in the text. (**B**) Formation of DCF (relative pixel intensity) from DCFH$_2$-DA (100 μM) in HepG2 cells during 30 min of reoxygenation following 4 h of anoxia and incubation with DCFH$_2$-DA under anoxic conditions (A/R, blue line) or similar procedures in the presence of the antioxidant dimethyl malonate during the anoxia period (A/R + DMM, red line). Control cells were perfused and incubated with DCFH$_2$-DA under normoxic conditions (4 h perfusion followed by 30 min imaging; control, green line). Data (n = 3/group) are presented as mean ± SEM. Representative fluorescence microscopy images of the data presented in (**B**) are shown for reperfused cells following (**C**) anoxia, (**D**) reperfusion following anoxia + DMM, and (**E**) control conditions.

Addition of 1 mM DMM to the perfusion and incubation medium resulted in a profound decrease in DCF formation during reoxygenation (Figure 6C,D). Considering that the effect of DMM stems from a reduction in succinate accumulation during anoxia that hampers mitochondrial oxidant formation upon reoxygenation [33], the increase in DCF fluorescence during A/R most likely resulted from mitochondrial oxidative stress that manifests in the cytosol where mitochondria-derived oxidants react with DCFH$_2$. In that respect, the maximum signal intensity observed at t ~10 min indicates that mitochondrial

oxidant formation during A/R is a rapid yet short-lived effect, as has previously been postulated in the context of hepatic ischemia-reperfusion [32].

4. Discussion

The main limitations for the use of $DCFH_2$-DA in experiments with HepG2 and HepaRG cells are uptake of extracellular DCF, poor DCF retention, and cell type-specificity of $DCFH_2$ oxidation under resting conditions. $DCFH_2$-DA stability is notably affected by the type and pH of incubation medium in which it is dissolved. Nevertheless, $DCFH_2$-DA can be a useful means to analyze general oxidative stress in HepG2 and HepaRG cells granted that the experimental setup accounts for these limitations. A schematic overview of an experimental setup that aims to optimize conditions for the use of $DCFH_2$-DA in cells of hepatocellular origin is presented in Figure 7.
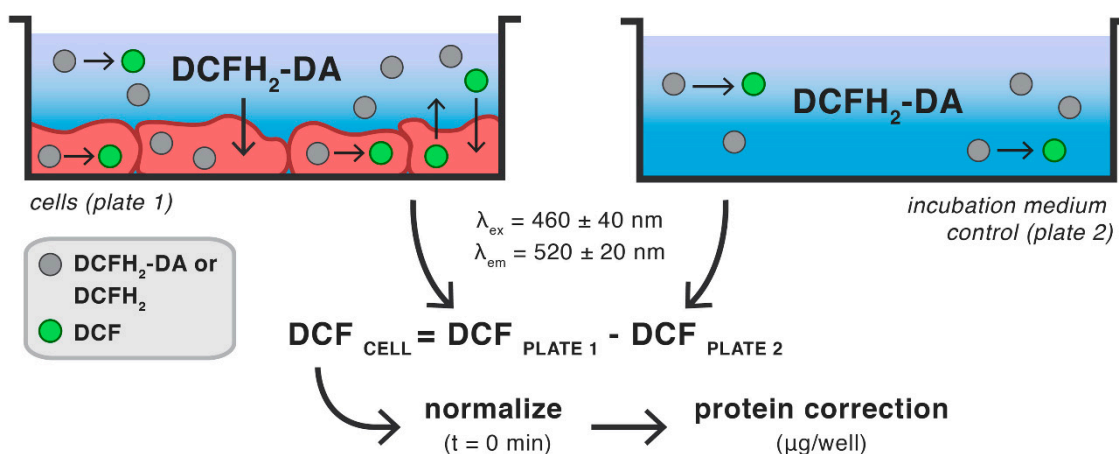
Figure 7. Schematic overview of optimized assay conditions for the use of $DCFH_2$-DA in cultured hepatocytes. Details are provided in the text.

The incubation medium should preferably contain ≥ 60 µM $DCFH_2$-DA in either PBS or serum-free WE or RPMI medium, which needs to be HEPES-buffered when performing experiments at ambient CO_2 tension to maintain pH. The assay is ideally performed in a fluorescence microplate reader (equilibrated to 37 °C) in time-based acquisition mode and equipped with the appropriate filters for DCF fluorescence detection (e.g., $\lambda_{ex} = 460 \pm 40$, $\lambda_{em} = 520 \pm 20$ nm). Directly following analysis of the assay plate, a second plate containing only incubation medium (exactly corresponding to that used in the assay plate) should be read to correct for extracellular DCF formation. The raw data from the cell-free plate (2) need to be subtracted from the corresponding wells of the assay plate (1) at each individual time point to calculate cellular DCF fluorescence (Figure 7, equation). Sample a.u. values should be close to 0 for the baseline measurement following this step, as was the case with the data presented in Figure 5. However, if considerable differences in baseline values prevail, for instance due to a significant time lag in pipetting the incubation medium, data can be additionally normalized by subtracting the raw data at baseline (first read) from every subsequent time point per sample (Figure 7, normalize). Irrespective of whether baseline correction is performed, each data point should be normalized to the total protein (or DNA) content per well to correct for differences in seeding density (Figure 7, protein correction).

By incubating the cells with $DCFH_2$-DA throughout the assay period, intracellular $DCFH_2$(-DA) levels are maintained constantly. Moreover, intracellularly generated DCF that is expelled into the extracellular space will be detected, whilst outcomes are corrected for DCF formation in the incubation medium. In doing so, $DCFH_2$-DA can be used to generate data on intracellular oxidative stress with minimal interference. This approach could be useful when $DCFH_2$-DA, as well as other fluorogenic probes with similar properties

(e.g., dihydrorhodamine 123 and hydroethidine [53]), are used on cell lines that express membrane transport proteins, such as MRP1-expressing RAW 264.7 macrophages [53].

There are limitations to $DCFH_2$-DA that are more cumbersome to correct for. Specifically, $DCFH_2$ oxidation involves the formation of an intermittent radial species, the DCF semiquinone radical ($DCF^{\bullet}/DCF^{\bullet-}$) [13,14], which could affect DCF formation via both direct, i.e., $DCFH_2$ oxidation, and indirect, i.e., $O_2^{\bullet-}$ formation, mechanisms [7,13]. In addition, overoxidation of DCF into nonfluorescent degradation products could lead to an underestimation of DCF formation [7]. Although these phenomena are not specific to $DCFH_2$-DA [7], it will be difficult to quantify the full extent to which these processes contribute to DCF formation under assay conditions and to correct for them experimentally. A second, more relative limitation of $DCFH_2$(-DA) is its non-specificity towards various radical and non-radical oxidants [9–12]. It is therefore suggested to regard data generated using $DCFH_2$-DA as a measure for overall 'oxidative' or 'redox stress' and to avert to more specific probes (e.g., hydroethidine or Amplex Red) or techniques (e.g., electron paramagnetic resonance) when detection of particular radical or oxidant species is warranted.

In addition to the experimental setup presented in Figure 7, the probe can be also used to visualize and quantify cytosolic oxidative stress during A/R in real time. This technique can for example be employed to analyze the direct effect of pharmacological interventions that target intracellular oxidative stress or to analyze other phenomena using different dyes (e.g., JC-1 for mitochondrial membrane potential analysis), further expanding the possible applications of $DCFH_2$-DA.

5. Conclusions

Despite its limitations $DCFH_2$-DA can function as a useful fluorogenic probe to investigate the intracellular redox state in the context of liver disease. Experimental setups are proposed that circumvent most of the interfering factors. Nevertheless, caution should always be taken when interpreting data generated using fluorogenic redox probes as it is not possible to correct for all limitations.

Data Availability Statement: Data is contained within the article and supplementary material.

Conflicts of Interest: The authors declare no conflict of interest.

References

1. Reiniers, M.J.; van Golen, R.F.; van Gulik, T.M.; Heger, M. Reactive oxygen and nitrogen species in steatotic hepatocytes: A molecular perspective on the pathophysiology of ischemia-reperfusion injury in the fatty liver. *Antioxid Redox Signal* **2014**, *21*, 1119–1142. [CrossRef]
2. Zangar, R.C.; Davydov, D.R.; Verma, S. Mechanisms that regulate production of reactive oxygen species by cytochrome P450. *Toxicol. Appl. Pharmacol.* **2004**, *199*, 316–331. [CrossRef] [PubMed]
3. Turrens, J.F. Mitochondrial formation of reactive oxygen species. *J. Physiol* **2003**, *552 Pt 2*, 335–344. [CrossRef]
4. Kakhlon, O.; Cabantchik, Z.I. The labile iron pool: Characterization, measurement, and participation in cellular processes (1). *Free Radic. Biol. Med.* **2002**, *33*, 1037–1046. [CrossRef]
5. Bedard, K.; Krause, K.H. The NOX family of ROS-generating NADPH oxidases: Physiology and pathophysiology. *Physiol. Rev.* **2007**, *87*, 245–313. [CrossRef]
6. Kloek, J.J.; Marechal, X.; Roelofsen, J.; Houtkooper, R.H.; van Kuilenburg, A.B.; Kulik, W.; Bezemer, R.; Neviere, R.; van Gulik, T.M.; Heger, M. Cholestasis is associated with hepatic microvascular dysfunction and aberrant energy metabolism before and during ischemia-reperfusion. *Antioxid. Redox Signal* **2012**, *17*, 1109–1123. [CrossRef]
7. Wardman, P. Fluorescent and luminescent probes for measurement of oxidative and nitrosative species in cells and tissues: Progress, pitfalls, and prospects. *Free Radic. Biol. Med.* **2007**, *43*, 995–1022. [CrossRef]
8. Gomes, A.; Fernandes, E.; Lima, J.L. Fluorescence probes used for detection of reactive oxygen species. *J. Biochem. Biophys. Methods* **2005**, *65*, 45–80. [CrossRef]
9. Wrona, M.; Patel, K.; Wardman, P. Reactivity of 2′,7′-dichlorodihydrofluorescein and dihydrorhodamine 123 and their oxidized forms toward carbonate, nitrogen dioxide, and hydroxyl radicals. *Free Radic. Biol. Med.* **2005**, *38*, 262–270. [CrossRef] [PubMed]
10. Reiniers, M.J.; van Golen, R.F.; Bonnet, S.; Broekgaarden, M.; van Gulik, T.M.; Egmond, M.R.; Heger, M. Preparation and Practical Applications of 2′,7′-Dichlorodihydrofluorescein in Redox Assays. *Anal. Chem.* **2017**, *89*, 3853–3857. [CrossRef]
11. Wrona, M.; Patel, K.B.; Wardman, P. The roles of thiol-derived radicals in the use of 2′,7′-dichlorodihydrofluorescein as a probe for oxidative stress. *Free Radic. Biol. Med.* **2008**, *44*, 56–62. [CrossRef]
12. Burkitt, M.J.; Wardman, P. Cytochrome C is a potent catalyst of dichlorofluorescin oxidation: Implications for the role of reactive oxygen species in apoptosis. *Biochem. Biophys. Res. Commun.* **2001**, *282*, 329–333. [CrossRef] [PubMed]
13. Rota, C.; Chignell, C.F.; Mason, R.P. Evidence for free radical formation during the oxidation of 2′-7′-dichlorofluorescin to the fluorescent dye 2′-7′-dichlorofluorescein by horseradish peroxidase: Possible implications for oxidative stress measurements. *Free Radic. Biol. Med.* **1999**, *27*, 873–881. [CrossRef]
14. Wrona, M.; Wardman, P. Properties of the radical intermediate obtained on oxidation of 2′,7′-dichlorodihydrofluorescein, a probe for oxidative stress. *Free Radic. Biol. Med.* **2006**, *41*, 657–667. [CrossRef]
15. Mchedlov-Petrossyan, N.O.; Rubtsov, M.I.; Lukatskaya, L.L. Ionization and tautomerism of chloro-derivatives of fluorescein in water and aqueous acetone. *Dyes. Pigm.* **1992**, *18*, 179–198. [CrossRef]
16. Hafer, K.; Iwamoto, K.S.; Schiestl, R.H. Refinement of the dichlorofluorescein assay for flow cytometric measurement of reactive oxygen species in irradiated and bystander cell populations. *Radiat. Res.* **2008**, *169*, 460–468. [CrossRef] [PubMed]
17. Hempel, S.L.; Buettner, G.R.; O'Malley, Y.Q.; Wessels, D.A.; Flaherty, D.M. Dihydrofluorescein diacetate is superior for detecting intracellular oxidants: Comparison with 2′,7′-dichlorodihydrofluorescein diacetate, 5(and 6)-carboxy-2′,7′-dichlorodihydrofluorescein diacetate, and dihydrorhodamine 123. *Free Radic. Biol. Med.* **1999**, *27*, 146–159. [CrossRef]
18. Karlsson, M.; Kurz, T.; Brunk, U.T.; Nilsson, S.E.; Frennesson, C.I. What does the commonly used DCF test for oxidative stress really show? *Biochem. J.* **2010**, *42*, 183–190. [CrossRef]
19. Keller, A.; Mohamed, A.; Drose, S.; Brandt, U.; Fleming, I.; Brandes, R.P. Analysis of dichlorodihydrofluorescein and dihydrocalcein as probes for the detection of intracellular reactive oxygen species. *Free Radic. Res.* **2004**, *38*, 1257–1267. [CrossRef]
20. LeBel, C.P.; Ischiropoulos, H.; Bondy, S.C. Evaluation of the probe 2′,7′-dichlorofluorescin as an indicator of reactive oxygen species formation and oxidative stress. *Chem. Res. Toxicol.* **1992**, *5*, 227–231. [CrossRef]
21. Myhre, O.; Andersen, J.M.; Aarnes, H.; Fonnum, F. Evaluation of the probes 2′,7′-dichlorofluorescin diacetate, luminol, and lucigenin as indicators of reactive species formation. *Biochem. Pharmacol.* **2003**, *65*, 1575–1582. [CrossRef]
22. Royall, J.A.; Ischiropoulos, H. Evaluation of 2′,7′-dichlorofluorescin and dihydrorhodamine 123 as fluorescent probes for intracellular H2O2 in cultured endothelial cells. *Arch. Biochem. Biophys.* **1993**, *302*, 348–355. [CrossRef]
23. Swift, L.M.; Sarvazyan, N. Localization of dichlorofluorescin in cardiac myocytes: Implications for assessment of oxidative stress. *Am. J. Physiol. Heart Circ. Physiol.* **2000**, *278*, H982–H990. [CrossRef] [PubMed]
24. Zhu, H.; Bannenberg, G.L.; Moldeus, P.; Shertzer, H.G. Oxidation pathways for the intracellular probe 2′,7′-dichlorofluorescein. *Arch. Toxicol.* **1994**, *68*, 582–587. [CrossRef] [PubMed]
25. Roth, M.; Obaidat, A.; Hagenbuch, B. OATPs, OATs and OCTs: The organic anion and cation transporters of the SLCO and SLC22A gene superfamilies. *Br. J. Pharmacol.* **2012**, *165*, 1260–1687. [CrossRef] [PubMed]
26. Gripon, P.; Rumin, S.; Urban, S.; Le Seyec, J.; Glaise, D.; Cannie, I.; Guyomard, C.; Lucas, J.; Trepo, C.; Guguen-Guillouzo, C. Infection of a human hepatoma cell line by hepatitis B virus. *Proc. Natl. Acad. Sci. USA* **2002**, *99*, 15655–15660. [CrossRef] [PubMed]

27. Poggendorff, J.C. *Annalen der Physik*. 1852. Available online: https://de.wikisource.org/wiki/Annalen_der_Physik (accessed on 5 January 2021).

28. Broekgaarden, M.; Weijer, R.; Krekorian, M.; van den Ijssel, B.; Kos, M.; Alles, L.K.; van Wijk, A.C.; Bikadi, Z.; Hazai, E.; van Gulik, T.M.; et al. Inhibition of hypoxia-inducible factor 1 with acriflavine sensitizes hypoxic tumor cells to photodynamic therapy with zinc phthalocyanine-encapsulating cationic liposomes. *Nano Res.* **2016**, *9*, 1639–1662. [CrossRef]

29. Weijer, R.; Broekgaarden, M.; Krekorian, M.; Alles, L.K.; van Wijk, A.C.; Mackaaij, C.; Verheij, J.; van der Wal, A.C.; van Gulik, T.M.; Storm, G.; et al. Inhibition of hypoxia inducible factor 1 and topoisomerase with acriflavine sensitizes perihilar cholangiocarcinomas to photodynamic therapy. *Oncotarget* **2016**, *7*, 3341–3356. [CrossRef]

30. van Raath, M.I.; Weijer, R.; Nguyen, G.H.; Choi, B.; de Kroon, A.I.; Heger, M. Tranexamic Acid-Encapsulating Thermosensitive Liposomes for Site-Specific Pharmaco-Laser Therapy of Port Wine Stains. *J. Biomed. Nanotechnol.* **2016**, *12*, 1617–1640. [CrossRef]

31. Heger, M.; Salles, I.I.; van Vuure, W.; Hamelers, I.H.; de Kroon, A.I.; Deckmyn, H.; Beek, J.F. On the interaction of fluorophore-encapsulating PEGylated lecithin liposomes with hamster and human platelets. *Microvasc. Res.* **2009**, *78*, 57–66. [CrossRef]

32. van Golen, R.F.; van Gulik, T.M.; Heger, M. Mechanistic overview of reactive species-induced degradation of the endothelial glycocalyx during hepatic ischemia/reperfusion injury. *Free Radic. Biol. Med.* **2012**, *52*, 1382–1402. [CrossRef]

33. Chouchani, E.T.; Pell, V.R.; Gaude, E.; Aksentijevic, D.; Sundier, S.Y.; Robb, E.L.; Logan, A.; Nadtochiy, S.M.; Ord, E.N.J.; Smith, A.C.; et al. Ischaemic accumulation of succinate controls reperfusion injury through mitochondrial ROS. *Nature* **2014**, *515*, 431–435. [CrossRef]

34. Grzelak, A.; Rychlik, B.; Bartosz, G. Light-dependent generation of reactive oxygen species in cell culture media. *Free Radic. Biol. Med.* **2001**, *30*, 1418–1425. [CrossRef]

35. Wardman, P.; Candeias, L.P. Fenton chemistry: An introduction. *Radiat. Res.* **1996**, *145*, 523–531. [CrossRef]

36. Hua Long, L.; Halliwell, B. Oxidation and generation of hydrogen peroxide by thiol compounds in commonly used cell culture media. *Biochem. Biophys. Res. Commun.* **2001**, *286*, 991–994. [CrossRef]

37. Long, L.H.; Halliwell, B. Artefacts in cell culture: Pyruvate as a scavenger of hydrogen peroxide generated by ascorbate or epigallocatechin gallate in cell culture media. *Biochem. Biophys. Res. Commun.* **2009**, *388*, 700–704. [CrossRef] [PubMed]

38. Kirsch, M.; Lomonosova, E.E.; Korth, H.G.; Sustmann, R.; de Groot, H. Hydrogen peroxide formation by reaction of peroxynitrite with HEPES and related tertiary amines. Implications for a general mechanism. *J. Biol. Chem.* **1998**, *273*, 12716–14724. [CrossRef]

39. Keynes, R.G.; Griffiths, C.; Garthwaite, J. Superoxide-dependent consumption of nitric oxide in biological media may confound in vitro experiments. *Biochem. J.* **2003**, *369*, 399–406. [CrossRef] [PubMed]

40. Edwards, A.M.; Silva, E. Effect of visible light on selected enzymes, vitamins and amino acids. *J. Photochem. Photobiol. B* **2001**, *63*, 126–131. [CrossRef]

41. Baker, C.J.; Mock, N.M.; Roberts, D.P.; Deahl, K.L.; Hapeman, C.J.; Schmidt, W.F.; Kochansky, J. Interference by Mes [2-(4-morpholino)ethanesulfonic acid] and related buffers with phenolic oxidation by peroxidase. *Free Radic. Biol. Med.* **2007**, *43*, 1322–1327. [CrossRef] [PubMed]

42. Zamek-Gliszczynski, M.J.; Xiong, H.; Patel, N.J.; Turncliff, R.Z.; Pollack, G.M.; Brouwer, K.L. Pharmacokinetics of 5 (and 6)-carboxy-2′,7′-dichlorofluorescein and its diacetate promoiety in the liver. *J. Pharmacol. Exp. Ther.* **2003**, *304*, 801–809. [CrossRef]

43. Chen, X.; Zhong, Z.; Xu, Z.; Chen, L.; Wang, Y. 2′,7′-Dichlorodihydrofluorescein as a fluorescent probe for reactive oxygen species measurement: Forty years of application and controversy. *Free Radic. Res.* **2010**, *44*, 587–604. [CrossRef]

44. Hart, S.N.; Li, Y.; Nakamoto, K.; Subileau, E.A.; Steen, D.; Zhong, X.B. A comparison of whole genome gene expression profiles of HepaRG cells and HepG2 cells to primary human hepatocytes and human liver tissues. *Drug Metab. Dispos.* **2010**, *38*, 988–994. [CrossRef]

45. Williams, F.M.; Mutch, E.; Blain, P.G. Esterase activity in rat hepatocytes. *Biochem. Pharmacol.* **1991**, *41*, 527–531. [CrossRef]

46. De Bruyn, T.; Fattah, S.; Stieger, B.; Augustijns, P.; Annaert, P. Sodium fluorescein is a probe substrate for hepatic drug transport mediated by OATP1B1 and OATP1B3. *J. Pharm. Sci.* **2011**, *100*, 5018–5030. [CrossRef] [PubMed]

47. Du, Y.; Han, R.; Ng, S.; Ni, J.; Sun, W.; Wohland, T.; Ong, S.H.; Kuleshova, L.; Yu, H. Identification and characterization of a novel prespheroid 3-dimensional hepatocyte monolayer on galactosylated substratum. *Tissue Eng.* **2007**, *13*, 1455–1468. [CrossRef] [PubMed]

48. Chahal, P.S.; Neal, M.J.; Kohner, E.M. Metabolism of fluorescein after intravenous administration. *Investig. Ophthalmol. Vis. Sci.* **1985**, *26*, 764–768.

49. Sabnis, R.W. *Handbook of Fluorescent Dyes and Probes*; John Wiley & Sons: Hoboken, NJ, USA, 2015.

50. Kachel, K.; Asuncion-Punzalan, E.; London, E. The location of fluorescence probes with charged groups in model membranes. *Biochim. Biophys. Acta* **1998**, *1374*, 63–76. [CrossRef]

51. Nibourg, G.A.; Chamuleau, R.A.; van Gulik, T.M.; Hoekstra, R. Proliferative human cell sources applied as biocomponent in bioartificial livers: A review. *Expert Opin. Biol. Ther.* **2012**, *12*, 905–921. [CrossRef]

52. Gasbarrini, A.; Borle, A.B.; Farghali, H.; Bender, C.; Francavilla, A.; Van Thiel, D. Effect of anoxia on intracellular ATP, Na+i, Ca2+i, Mg2+i, and cytotoxicity in rat hepatocytes. *J. Biol. Chem.* **1992**, *267*, 6654–6663. [CrossRef]

53. Prochazkova, J.; Kubala, L.; Kotasova, H.; Gudernova, I.; Sramkova, Z.; Pekarova, M.; Sarkadi, B.; Pachernik, J. ABC transporters affect the detection of intracellular oxidants by fluorescent probes. *Free Radic. Res.* **2011**, *45*, 779–787. [CrossRef] [PubMed]